Nuclear Inst. and Methods in Physics Research, A

Noise spectroscopy study of methylammonium lead tribromide single-crystal detectors: gamma spectroscopy applications

--Manuscript Draft--

Manuscript Number:	
Article Type:	Full length article
Section/Category:	Gamma, X-ray and Charged Particle Detectors
Keywords:	Lead halide perovskite; gamma-ray detector; noise power spectral density
Corresponding Author:	Eric Gros-Daillon, Ph.D. CEA-Leti: Commissariat a l'energie atomique et aux energies alternatives Laboratoire d'electronique et de technologies de l'information GRENOBLE, FRANCE
First Author:	Oriane Baussens
Order of Authors:	Oriane Baussens
	Guillaume Montémont
	Jean-Marie Verilhac
	Lionel Hirsch
	Eric Gros-Daillon
Abstract:	Metal halide perovskites have been studied since 2016 for gamma spectroscopy applications. In this work, we study devices based on methylammonium lead tribromide single crystals as gamma detectors. These detectors can measure the signal of a single gamma photon but the energy resolution is limited by the noise of the detectors. Such noise is multicomponent and a deeper investigation was carried by measuring the noise power spectral density of the devices for different bias voltages. Non-biased devices were found to behave as an idealized equivalent electrical circuit with the main noise source being thermal noise. In the case of biased devices, the dominant noise source is shown to be the 1/f noise which becomes preponderant at lower frequency (<1MHz). These results demonstrate the major contribution of the flicker noise in perovskite detectors and lay the foundation for next developments to make them compatible with spectrometric applications.
Suggested Reviewers:	Olivier Limousin, Ph.D. Research engineer, CEA IRFU: Commissariat a l'energie atomique et aux energies alternatives Institut de recherche sur les lois fondamentales de l'Univers olivier.limousin@cea.fr He is a specialist of spectroscopic imaging. He was also a reviewer for my thesis so he is already familiar the work submitted for publication.
	Paul Sellin, Ph.D Professor of Physics, University of Surrey p.sellin@surrey.ac.uk He is a specialist in semiconductor nuclear detectors and has studied both high Z classical semiconductors (CdTe, CZT...) and perovskites.
Opposed Reviewers:	

Powered by Editorial Manager® and ProduXion Manager® from Aries Systems Corporation

Noise spectroscopy study of methylammonium lead tribromide single-crystal detectors: gamma spectroscopy applications

O. Baussens[a], G. Montémont[a], JM. Verilhac[b], L. Hirsch[c], E. Gros-Daillon[a]

[a]University Grenoble Alpes, CEA, LETI, F38000 Grenoble, France
[b]University Grenoble Alpes, CEA, LITEN, F38000 Grenoble, France
[c]University Bordeaux, IMS-CNRS, UMR 5218, Bordeaux INP, ENSCBP, F33405 Talence, France

Author to whom correspondence should be addressed:
E. Gros-Daillon, eric.grosdaillon@cea.fr, CEA Grenoble 17 Avenue des Martyrs 38000 Grenoble, FRANCE.

***Abstract*—Metal halide perovskites have been studied since 2016 for gamma spectroscopy applications. In this work, we study devices based on methylammonium lead tribromide single crystals as gamma detectors. These detectors can measure the signal of a single gamma photon but the energy resolution is limited by the noise of the detectors. Such noise is multicomponent and a deeper investigation was carried by measuring the noise power spectral density of the devices for different bias voltages. Non-biased devices were found to behave as an idealized equivalent electrical circuit with the main noise source being thermal noise. In the case of biased devices, the dominant noise source is shown to be the 1/*f* noise which becomes preponderant at lower frequency (<1MHz). These results demonstrate the major contribution of the flicker noise in perovskite detectors and lay the foundation for next developments to make them compatible with spectrometric applications.**

***Index Terms*— Lead halide perovskite, gamma-ray detector, noise power spectral density.**

1 Introduction

Metal halide perovskites are a new type of material that has attracted the interest of the high energy radiation detection community for the past few years. The reasons behind this interest are the presence of heavy atoms, such as lead, in their composition, the high charge transport properties and the possibility to grow thick single crystals in solution at low temperature. Since 2016, studies have been conducted to measure the energy resolution of lead halide perovskites gamma detectors. An energy resolution of 10% FWHM at 59.5keV was demonstrated for cesium lead tribromide ($CsPbBr_3$) and methylammonium lead triiodide ($MAPbI_3$) single crystals using an americium source [1,2]. For the same gamma source, chloride doped methylammonium lead tribromide ($MAPbBr_{2.85}Cl_{0.15}$) single crystals showed an energy resolution of 35% FWHM [3]. More recently, an impressive energy resolution of 1.4% FWHM at 662keV has been demonstrated on detector based on Bridgman grown $CsPbBr_3$ crystals [4]. In addition to these proofs of concepts, it is of major importance to identify the limiting factors for the spectral resolution of lead halide perovskites. Noise in the detector and electronic noise in the readout circuit are important figures of merit affecting the energy resolution. In that respect, noise spectroscopy is a powerful tool standardly used for semiconductor detectors [5–7]. However, for perovskites single crystals, to the best of your knowledge, noise spectroscopy has only been used once, as a screening tool to differentiate samples with higher or lower spectrometric performances [8]. Here, we propose a more in-depth study focusing on determining the main components of perovskite single crystals noise spectra.

In this work, we study devices based on methylammonium lead tribromide ($MAPbBr_3$) single crystals crystallized from solution. The noise spectra of the devices have been analyzed as a function of applied voltages and the different root causes of noise have been identified. The aim is to understand which noise components tend to limit the gamma photon counting performances of the devices.

2 Methods

2.1 Crystal growth and device fabrication

The $MAPbBr_3$ single crystals were grown independently using seeded Inverse Temperature Crystallization method. The growth process is described in previous work [9]. Crystals dimensions after growth were 4mm × 4mm × 2mm on average. Their top and bottom (100) faces were optically polished (roughness below 30 nm r.m.s) and chromium electrodes were thermally evaporated on them through a shadow mask. After polishing, the average crystal thickness was 1mm.

2.1.1 Gamma photon counting

The photocurrent induced by gamma photons with energies ranging from 59.5keV to 511keV was measured using a homemade

Charge Sensitive Amplifier (Junction Field Effect Transistor, JFET 2SK715, input discrete CSA) and digitized with a *Tektronix* TDS220 oscilloscope. Two $MAPbBr_3$ pixelated devices were used for the measurement (pixel pitch: 600µm) to benefit from the small pixel effect [10]. The measurements were carried out under ambient temperature and humidity conditions. The device was placed in a brass casing, ensuring electromagnetic insulation as well as dark conditions. The minimum voltage bias required to ensure complete charge collection can be calculated from equation 1.

$$V_{min} = \frac{L^2}{\mu\tau} \tag{1}$$

L is the thickness of the device. μ is the mobility of the charge carriers and τ is their lifetime. The average thickness of our devices is 1mm. In a previous paper, the average holes' mobility was measured at $13cm^2.V^{-1}.s^{-1}$ using laser Transient Current Technique (TCT) [11]. In the same paper, the holes' lifetime was estimated to be above 10µs and the electrons' transport properties were hypothesized to be lower than the holes' transport properties. From these values, the minimum bias voltage to ensure that the majority of the charge carriers are collected is estimated at 80V for holes and should be higher to ensure complete charge collection of electrons. However, the devices were too noisy to reach this threshold and the measurements were conducted at 20V.

2.2 Noise spectroscopy measurements

2.2.1 Noise spectroscopy setup

The noise power spectral density (PSD) measurements were conducted on two $MAPbBr_3$ non-pixelated devices with 19.6 mm^2 and 5.6 mm^2 active surface for device 1 and 2 respectively (Table 1). The measurements took place under laboratory temperature (20°C-25°C) and humidity conditions (40%-60%RH).
Figure 1 shows the setup used for the noise spectroscopy measurements. The device to be measured was placed in a brass sample holder. The simplest electrical equivalent circuit model for the device is a resistor in parallel with a capacitance ($R_{dev}//C_{dev}$). Values for R_{dev} and C_{dev} are estimated in section 3.B.1. For the measurement, the device was biased using a *Keithley* SMU 2602B via resistor R_0 (470MΩ). The *Keithley* SMU 2602B was also used to measure the value of the dark current. The dark current of the device was amplified using a homemade charge sensitive amplifier (JFET input discrete CSA). The charge amplifier consisted of an amplification stage (G_1) and an impedance matching stage (G_2). A *Teledyne LeCroy* HDO6104 oscilloscope (1MΩ input impedance) then measured the amplified current and calculated the output noise power spectral density (Figure 2B).

The input noise PSD (Figure 2C) is obtained by performing the ratio between the output noise PSD and the gain of the charge amplifier.

$$PSD_{IN} = \frac{PSD_{OUT}}{Gain} \tag{2}$$

The gain spectrum of the charge amplifier was measured (Figure 2A) by simulating the charge that would be produced by a 511keV photon absorbed in $MAPbBr_3$. 511keV was used as a reference energy because it is the highest energy of the range of interest for gamma spectroscopy [12]. This allowed us to measure the gain spectrum with the highest signal to noise ratio.

$$Q = \frac{E_{ph}}{W_{\pm}} = 12fC \tag{3}$$

E_{ph} [eV] is the photon's energy. $W_{\pm}$=6.9eV [eV] is the pair production energy in $MAPbBr_3$ as defined by Klein equation [13]. This charge is produced using an *Agilent* 33250A function generator and an injection capacitance C_{inj} (1pF).

$$V_{inj} = \frac{Q}{C_{inj}} = 12mV \tag{4}$$

V_{inj} [V] is the amplitude of the sinusoidal functions generated by the *Agilent* 33250A. The functions were generated for frequencies varying between 2kHz and 20MHz, the range of interest for gamma spectroscopy. However, the low cutoff frequency of the charge sensitive amplifier is 10kHz so all the spectra were analyzed between 10kHz and 20MHz.

FIGURE1

Figure 1. Noise spectroscopy measurement setup

FIGURE2

Figure 2. A) Typical gain spectrum (feedback capacitance C_1=100fF). B) Typical output power spectral density. C) Typical input power spectral density. D) Input power spectral density theoretical model.

2.2.2 Theoretical model

The input noise PSD can be modeled using the algebraic expressions of the theoretical noise sources of the different constitutive elements of the system. The two main sources of noise are the MAPbBr3 device and the charge preamplifier.

The device noise can be broken down into two main components: the shot noise and the flicker noise (1/*f* noise). The shot noise is due to the discrete nature of electronic charge carriers, which are injected into a biased device by following a Poisson statistic. It is proportional to the of the dark current. When represented in current spectral density units [A²/Hz], the shot noise is a white noise. The flicker noise is inversely proportional to the frequency (1/*f*) when represented in current spectral density units [A²/Hz]. This 1/*f* noise is linked to random processes in the material. Example of which include fluctuations in the rate of generation and recombination of carriers, fluctuations in effective mobility in the material as well as trapping and de-trapping phenomena. The noise power spectral density of the device can be expressed as the sum of its shot and 1/*f* noises.

$$\gamma_{device} = 2qI_{dark} + \frac{I_f^2}{f} \left[\frac{A^2}{Hz}\right] \tag{5}$$

q is the elementary charge [C]. I_{dark} is the dark current of the device [A]. I_f is a constant linked to the 1/*f* noise of the device [A].

The noise of the amplification electronics is mainly related to the components located upstream of the charge preamplifier: the input resistor and the input transistor. The input resistor is the parallel resistor between R_{dev} and R_0. In what follows, it will be noted $R_{\parallel}$. The input resistor is a source of Johnson noise which is the noise produced by the thermal agitation of charge carriers.

$$\gamma_{R\parallel} = \frac{4kT}{R_{\parallel}} \tag{6}$$

k [J.K^{-1}] is the Boltzmann constant. T [K] is the temperature.
The noise of the input transistor has two components: the shot noise and the 1/*f* noise. The shot noise of the transistor is white when represented in voltage spectral density units [V²/Hz]. The noise power spectral density of the input transistor can be expressed as the sum of its shot and 1/*f* noises.

$$\gamma_{transistor} = \frac{4kT}{g} + \frac{A_f}{f} \left[\frac{V^2}{Hz}\right] \tag{7}$$

g [S] is the transconductance of the amplification transistor. Its value is estimated in part 3.2.2 A_f [V²] is a constant linked to the technology of transistor used.

The contribution of all the noise sources mentioned leads to a global noise power spectral density (Figure 2D), expressed in charge spectral unit, as follows:

$$\gamma(f) = C^2 \times (\gamma_{transistor}) + \frac{1}{4\pi^2 f^2}(\gamma_{R\parallel} + \gamma_{device}) \left[\frac{C^2}{Hz}\right] \tag{8}$$

C [F] is the composed capacitance of the spectroscopic chain. It is the sum of the device capacitance (C_{dev}), the injection capacitance (C_{inj}=1pF), the charge amplifier feedback capacitance (C_1=0.1pF) and the stray capacitance (C_s). The stray capacitance is estimated in part 3.2.2 The composed capacitance is the factor that allows the conversion of the input transistor PSD from voltage units to charge units. The input resistors and device noise PSDs are multiplied by the factor $1/4\pi^2 f^2$ to convert them from current units to charge units.

3 Results

3.1 Gamma photons counting

Figure 3 shows gamma photons counting for americium 241 and cobalt 57 sources. The devices were able to distinguish single gamma photons of 59.5keV and 122 keV, but the signal is highly noisy which limits the energy resolution. The noise must be finely characterized in order to define a signal shaping that would be a good enough compromise between the reduction of the noise and the ballistic deficit. Furthermore, the origin of the noise has yet to be established.

FIGURE 3

Figure 3. Gamma photons counting of ^{241}Am and ^{57}Co gamma sources.

3.2 Noise spectroscopy measurements

3.2.1 Devices' properties

Table 1 gathers the main properties of the two devices used to conduct the noise spectroscopy measurements.

Table 1. Properties of the two devices used for noise spectroscopy measurements.

Device number	Length (mm)	Width (mm)	Thickness (mm)	Electrode surface (mm²)	Capacitance (pF)	Resistance (MΩ)
1	5.7	4.8	0.88	19.6	15±2.4	13±4

2	4.1	2.5	1.2	5.6	3.1±0.5	150±19

The value of the resistance of device 1 was measured using impedance spectroscopy measurements in a previous publication [14].The value of the resistance of device 2 was calculated using the value of conductivity estimated from same reference. The device's capacitances C_{dev} are estimated using the formula for planar capacitance.

$$C_{dev} = \frac{\varepsilon_0 \varepsilon_r S}{L} [F] \quad (9)$$

ε_0=8.85×10^{-12}F.m^{-1} is the dielectric constant. ε_r=76±11 is the dielectric permittivity of $MAPbBr_3$ [14]. S [m²] is the electrode's surface of the device. L [m] is the thickness of the device.

3.2.2 Estimation of the stray capacitance and the transconductance of the input transistor

The stray capacitance and the transconductance of the input transistor are estimated using equation 8 and noise PSD data measured at 10MHz without any device.

For high frequencies (10MHz), equation 8 can be simplified as follows.

$$\gamma(f = 10\text{MHz}) = (C_{inj} + C_1 + C_s)^2 \times \frac{4kT}{g} \left[\frac{V^2}{Hz}\right] \quad (10)$$

We hypothesize that the stray capacitance does not depend on the injection capacitance. The noise PSD is measured experimentally at 10MHz for two different injection capacitances: C_A=1pF and C_B=3.2pF. Values measured for each capacitance are 3.1×10^{-41} C²/Hz and 4.2×10^{-41} C²/Hz respectively. This leads to an estimated stray capacitance C_s=13.4pF and an estimated JFET transconductance g=110ms. The value of the transconductance was also estimated via a PSpice simulation (I_{drain}=10mA). The result of the simulation gave g=67mS. In what follows, we consider that possible values for the input transistor's transconductance are in a range of 67ms to 110mS.

3.2.3 Noise spectroscopy measurements of non-biased devices

The noise PSD of the non-biased devices were measured and compared with the experimental noise PSD of their ideal electronic equivalent circuits (R_{dev}//C_{dev}). The ideal electronic equivalent circuit of each device were made using discrete resistors and capacitors and measured following the procedure described in part 2.3.1. The noise PSD of the non-biased devices were also compared with the theoretical model introduced in part 2.3. Figure 4 shows these comparisons. Parameters used for the models shown in Figure 4 are summarized in Table 2.

FIGURE 4

Figure 4. Comparison of the noise PSD of the non-biased $MAPbBr_3$ with the noise PSD of its ideal equivalent electrical circuit and the theoretical model. A) Device 1. B) Device 2.

Table 2. Parameters for the models shown in Figure 4.

Model	C (pF)	g (mS)	A_f (pV²)	R_0 (MΩ)	R_{dev} (MΩ)	$R_{\parallel}$ (MΩ)
Charge Sensitive Amplifier only	14.5	85	0.12	470	-	470
Equivalent circuit of device 1	32.5	85	0.12	470	13	12.7
Equivalent circuit of device 2	18.1	85	0.12	470	150	114

Both devices (experimental data in black) behave similarly to their ideal electronic equivalent circuit (experimental data in grey, modeled data in red) and derive significantly from the baseline theoretical model of the charge sensitive amplifier noise spectrum (in yellow). There are two differences between the yellow and red models. The first is the addition of the capacitance of the device C_{dev} to the composed capacitance C, which shifts the spectrum upward to higher noise values. The second is the addition of the device resistor R_{dev}, which decreases $R_{\parallel}$, and thus increases the noise in the low frequency range (<1MHz).

For non-biased devices, the noise mainly comes from the input resistors and the input transistor of the CSA, with the main contributions being the Johnson noise and shot noise of the input transistor respectively at low (<1MHz) and high (>1MHz) frequencies. The Johnson noise is mainly due to the bulk resistance associated with thermally generated carriers ($R_{\parallel} \approx R_{device}$) while the shot noise of the input transistor is scaled by the composed capacitance.

3.2.4 *Noise spectroscopy measurement of biased devices*

3.2.4.1 *Noise spectroscopy as a function of bias voltage*

The noise PSD of both devices were measured for biases ranging between 0V and -90V using 10V steps (Figure 5). The values of the noise PSD measured at 10kHz are reported in the insert as a function of bias voltages.

FIGURE 5

Figure 5. Noise PSD spectra of device 1 (A) and 2 (B) as a function of bias voltages. In inserts, noise PSD at 10kHz as a function of bias voltage. The color code for bias values of the main graphs is kept in the inserts. The solid line in each insert represents the contribution of the shot noise of each device (which is proportional to the dark current) to the values of their respective noise PSD.

As expected from equation 8, at high frequency (f>1MHz), the noise PSD of both devices is a constant of the frequency and the bias voltage. The noise PSD only depends on the input transistor's transconductance and the composed capacitance. Similarly to the non-biased devices, the main noise source at high frequency is the shot noise of the input transistor of the charge sensitive amplifier.

At low frequency (f<1MHz), when the devices are biased we expect to see the addition of the device noise (both shot noise and $1/f$ noise) to the Johnson noise that was already present when the devices were not biased.

The inserts of Figure 5 give a simplified vision by showing only the noise PSD at 10kHz as a function of the bias voltage. It appears that the noise PSD increases with the bias voltage by following a quasi-linear trend. This trend may be expected if we consider that the dark current, from which the shot noise of the device depends, is proportional to the bias voltage. However, the spurious points seem to indicate transient phenomena. This invalidates the direct proportionality of the dark current with the bias voltage. Nevertheless, we cannot exclude that erratic migration phenomena may appear and generate some off-trend measurements [14].

Moreover, the values of dark currents measured lead to noise PSD (solid lines) lower than experimentally measured values (dots). The contribution of the shot noise from the devices to the noise PSD cannot explain the observed trend on its own.

3.2.4.2 *Frequency component analysis and modeling*

In order to figure out the relative extent of the contribution of the shot and $1/f$ noise of the device to the noise PSD at low frequency, we have performed a slope analysis on the noise PSD spectra shown in Figure 5. Each slope that make up the experimental spectra can be associated with one or more noise components. Looking at equation 11, which is the developed form of equation 8, we see that the noise components can be divided up into four categories in terms of their proportionality relationship with the frequency. Firstly, the shot noise of the input transistor (in grey) is independent of the frequency. It is associated with a constant slope. Secondly, the $1/f$ noise of the input transistor (in red) is proportional to the inverse of the frequency. It is associated with a -1 slope. Thirdly, the Johnson noise and the shot noise of the device are both proportional to $1/f^2$. They are associated with a -2 slope. Finally, the $1/f$ noise of the device (in blue) is proportional to $1/f^3$ so it is associated with a -3 slope.

$$\gamma(f) = C^2 \times \frac{4kT}{g} + C^2 \times \frac{A_f}{f} + \frac{1}{4\pi^2 f^2} \times \frac{4kT}{R_{\parallel}} + \frac{1}{4\pi^2 f^2} \times 2qI_{dark} + \frac{I_f^2}{4\pi^2 f^3} \quad \left[\frac{C^2}{Hz}\right] \tag{11}$$

The results of the slope analysis are summarized in Figure 6. Figure 6 A and B show the results for non-biased device 1 and 2 respectively. Graphs C and D show the results for biased (-20V) device 1 and 2 respectively. We notice the slope observed for biased devices were always the same regardless of the bias voltage applied.

Without biasing, both devices showed the same two main frequency components: a $1/f^2$ slope and a constant slope. From part 3.2.3, we deduce that these components correspond to the Johnson noise and the shot noise of the input transistor respectively.

For all non-zero biases tested, both devices showed the same two main frequency components in their PSD: a $1/f^3$ slope and a constant slope. This indicates that, for biased devices, the main noise sources are the $1/f$ noise of the device at low frequency (<1MHz) and the shot noise of the input transistor of the charge sensitive amplifier at high frequency (>1MHz).

FIGURE 6

Figure 6. Slope analysis of the noise PSD of the $MAPbBr_3$. A) Device 1 without biasing. B) Device 2 without biasing. C) Device 1 biased at -20V. D) Device 2 biased at -20V.

A quantitative analysis of the noise contributions for both devices is given in Figure 7. The analysis is performed for -20V bias voltage but the results remain the same for all non-zero bias voltages. The experimental data is represented with dots while the model based on equation 8 is represented with a solid black line. The contribution of each noise sources from the model is shown with colored solid lines. The value of I_f is adjusted to fit the noise PSD at low frequency. Looking at the contribution of each noise source, it appears that the shot noise gives rise to higher modeled values than experimental ones for mid-range frequencies (50kHz<f<1MHz). This leads to a deviation of the total model from the experimental data in that frequency range. The actual contribution of the dark current to the noise PSD is lower than expected.

FIGURE 7

Figure 7. Modeling of the noise PSD of device 1 (A) and 2 (B) biased at -20V. Experimental data are represented by dots. A black solid line represents the total model. The contribution of the noise sources to the total model are represented with colored solid lines.

A possible explanation could be the noise softening by the superficial trapping of the charge carriers [15]. The traps in the device can fragment the transit of the charge carriers. If charge carriers are trapped during their transit and then detrapped with a time constant of the order of the transit, the two portions of transit are independent. In that case, everything happens as if the charge carriers carried a charge lower than the elementary charge. This leads to lower shot noise and higher $1/f$ noise.
Figure 8 represents the modeling of the experimental data considering the hypothesis of noise softening via one superficial trapping level defined by a trapping constant τ. This hypothesis translates into the equation of the power spectral density of the device (equation 8) by adding a multiplying factor to the shot noise of the device as expressed in equation 12.

$$\gamma_{device} = 2qI_{dark} \times \frac{1}{1+(2\pi f\tau)^2} + \frac{I_f^2}{f} \left[\frac{A^2}{Hz}\right] \quad (12)$$

The modeling is performed for -20V bias voltage but the results remain the same for all non-zero bias voltages. The experimental data is represented with dots while the model based on equations (8) and (12) is represented with a solid black line. The contribution of each noise sources from the model is shown with colored solid lines. The parameters τ and I_f are optimized to fit the experimental data. The optimized values are 3µs and 0.25pV^2 respectively. All the parameters used are reported in the legend of Figure 8. The hypothesis of noise softening leads to a more convincing fit of the experimental data in the mid frequency-range.

FIGURE 8

Figure 8: Modeling of the noise PSD of device 1 (A) and 2 (B) biased at -20V using the hypothesis of the noise softening by the superficial trapping of the charge carriers. Experimental data are represented by dots. A black solid line represents the total model. The contribution of the noise sources to the total model are represented with colored solid lines.

4 Discussion

In the context of gamma photons counting, the frequency of interest for the measurement is the frequency associated with the transit time of the charge carriers generated by the photons inside the device. We have shown previously that holes have higher transport properties than electrons in $MAPbBr_3$ [11]. In this context and as a case study, we consider a pixelated device in hole collection mode only. The maximum transit time of holes is the time necessary for a hole generated near the anode to transit through the entire thickness of the device in order to reach the cathode. The transit time depends on the electric field in the device. In the hypothesis of a constant electric field inside the device, the transit time (t_t) can be estimated using the following equation.

$$t_t = \frac{L^2}{\mu_h V} [s] \quad (13)$$

L is the thickness of the device, about 1mm. μ_h is the mobility of holes which is, on average, 13cm^2.V^{-1}.s^{-1} [11]. V is the bias applied to the device. Ideally, this bias should be high enough for the transit time of the charge carriers to be much smaller than their lifetime. However, the higher the bias applied, the higher the dark current and the higher the shot noise of the device. In the case of the gamma photons counting measurements presented in Figure 3, the bias had to be limited to 20V in order to limit the noise enough so that the signal induced by the photons could be measured. The maximum transit time for a bias of 20V is about 30µs which corresponds to 5kHz. At this frequency, the main source of noise is the $1/f$ noise of the device.
It is an unfavorable condition, since the frequency of interest for the measurement correspond to high values of noise. However, an appropriate shaping of the signal might still allow for a favorable signal to noise ratio. Let us consider a RC-CR filter of the second order with a time constant of 30µs and estimate the equivalent noise charge (ENC) of the thus shaped signal.
The power spectral density of the filter can be expressed as follows.

$$\gamma_{filter} = \frac{(2\pi f)^2 {\tau_{filter}}^2}{\left(1+(2\pi f)^2 {\tau_{filter}}^2\right)^{n+1}} \quad (14)$$

τ_{filter} is the time constant of the filter (τ_{filter}=30µs) and n is its order (n=2).
The ENC^2 is the integral of the product of the input PSD (equations 8 and 12) and the PSD of the filter (equation 13). It is expressed as follows.

$$ENC^2 = 2\pi n \times \int \gamma_{filter}(f) \times \gamma(f) df \ [C^2] \quad (15)$$

The ENC for device 1 and 2 to have been estimated to be 132keV and 80keV FWHM respectively. This means that, even with an appropriate shaping, the noise is expected to be significant compared to energies of gamma photons equal to and below 150keV.

In order to increase the signal to noise ratio, it is mandatory to increase the charge carriers' mobility or to decrease the dark current through bulk resistivity increasing or electrode engineering [16].

5 Conclusion

The noise power spectral densities of $MAPbBr_3$ devices and their spectral chain were measured to uncover the main noise sources that limit the energy resolution of gamma photon counting measurements. For non-biased devices, we found that the main noise source is thermal noise from the resistances of the devices. However, when the devices are biased, the noise is dominated by the $1/f$ noise of the devices at low frequency (<1MHz). To our knowledge, this is the first results that highlighted the major contribution of flicker noise in thick hybrid perovskite detectors used for radiation detection. Further research will need to focus on the comprehension of the physical phenomena responsible for this $1/f$ noise in the devices. Moreover, the chosen theoretical model overvalues the contribution of the shot noise of the device to the total noise and leads to modeled values higher than experimental values in the mid frequency-range. We hypothesize that this observation could be explained by the noise softening via the superficial trapping of the charge carriers. Identifying and decreasing the noise of detectors is of major importance to improve their performances. This study provides new elements to guide the future developments of perovskite detectors for gamma-ray spectrometry.

6 Acknowledgements

This research was supported by ATTRACT project (PerXI) funded by the EC under Grant Agreement 777222. This research was also supported by the internal CEA project Hyster from the transverse instrumentation and detection skills program. This research was also supported by Trixell. The authors would like to thank Smaïl Amari for MAPbBr3 single-crystals fabrication, Marian Chapran for electrodes deposition, Julien Routin for his support on PCB hybridization and Adélie Presoz for her support on measurement during her internship.

References

[1] Y. He, L. Matei, H.J. Jung, K.M. McCall, M. Chen, C.C. Stoumpos, Z. Liu, J.A. Peters, D.Y. Chung, B.W. Wessels, M.R. Wasielewski, V.P. Dravid, A. Burger, M.G. Kanatzidis, High spectral resolution of gamma-rays at room temperature by perovskite CsPbBr 3 single crystals, Nat. Commun. 9 (2018) 1–8. https://doi.org/10.1038/s41467-018-04073-3.

[2] Y. He, W. Ke, G.C.B. Alexander, K.M. McCall, D.G. Chica, Z. Liu, I. Hadar, C.C. Stoumpos, B.W. Wessels, M.G. Kanatzidis, Resolving the Energy of γ-Ray Photons with MAPbI3 Single Crystals, ACS Photonics. 5 (2018) 4132–4138. https://doi.org/10.1021/acsphotonics.8b00873.

[3] J.T. Tisdale, M. Yoho, H. Tsai, S. Shrestha, K. Fernando, J.K. Baldwin, S. Tretiak, D. Vo, W. Nie, Methylammonium Lead Tribromide Single Crystal Detectors towards Robust Gamma-Ray Photon Sensing, Adv. Opt. Mater. 8 (2020) 2000233. https://doi.org/10.1002/adom.202000233.

[4] Y. He, M. Petryk, Z. Liu, D.G. Chica, I. Hadar, C. Leak, W. Ke, I. Spanopoulos, W. Lin, D.Y. Chung, B.W. Wessels, Z. He, M.G. Kanatzidis, CsPbBr3 perovskite detectors with 1.4% energy resolution for high-energy γ-rays, Nat. Photonics. 15 (2021) 36–42. https://doi.org/10.1038/s41566-020-00727-1.

[5] G. Bertuccio, G. Ferrari, P. Gallina, M. Sampietro, E. Caroli, A. Donati, W. Dusi, Experimental analysis of current noise spectra in CdTe detectors, in: Hard X-Ray Gamma-Ray Neutron Detect. Phys., SPIE, 1999: pp. 402–408. https://doi.org/10.1117/12.366606.

[6] J. Sikula, L. Stourac, Noise spectroscopy of semiconductor materials and devices, in: 2002 23rd Int. Conf. Microelectron. Proc. Cat No02TH8595, 2002: pp. 767–772 vol.2. https://doi.org/10.1109/MIEL.2002.1003370.

[7] G. Montemont, J.-P. Rostaing, L. Verger, Experimental comparison of discrete and CMOS charge sensitive preamplifiers for CZT radiation detectors, IEEE Trans. Nucl. Sci. 50 (2003) 936–941. https://doi.org/10.1109/TNS.2003.815110.

[8] Z. Liu, J.A. Peters, J.I. Kim, S. Das, K.M. McCall, B.W. Wessels, Y. He, W. Lin, M.G. Kanatzidis, Noise sources and their limitations on the performance of compound semiconductor hard radiation detectors, Nucl. Instrum. Methods Phys. Res. Sect. Accel. Spectrometers Detect. Assoc. Equip. 916 (2019) 133–140. https://doi.org/10.1016/j.nima.2018.11.013.

[9] S. Amari, J.-M. Verilhac, E. Gros D'Aillon, A. Ibanez, J. Zaccaro, Optimization of the growth conditions for high quality CH3NH3PbBr3 hybrid perovskite single crystals, Cryst. Growth Des. (2020). https://doi.org/10.1021/acs.cgd.9b01429.

[10] H.H. Barrett, J.D. Eskin, H.B. Barber, Charge Transport in Arrays of Semiconductor Gamma-Ray Detectors, Phys. Rev. Lett. 75 (1995) 156–159. https://doi.org/10.1103/PhysRevLett.75.156.

[11] O. Baussens, L. Maturana, S. Amari, J. Zaccaro, J.-M. Verilhac, L. Hirsch, E. Gros-Daillon, An insight into the charge carriers transport properties and electric field distribution of CH3NH3PbBr3 thick single crystals, Appl. Phys. Lett. 117 (2020) 041904. https://doi.org/10.1063/5.0011713.

[12] L. Verger, E. Gros d'Aillon, O. Monnet, G. Montémont, B. Pelliciari, New trends in γ-ray imaging with CdZnTe/CdTe at CEA-Leti, Nucl. Instrum. Methods Phys. Res. Sect. Accel. Spectrometers Detect. Assoc. Equip. 571 (2007) 33–43.

https://doi.org/10.1016/j.nima.2006.10.023.
[13] C.A. Klein, Bandgap Dependence and Related Features of Radiation Ionization Energies in Semiconductors, J. Appl. Phys. 39 (1968) 2029–2038. https://doi.org/10.1063/1.1656484.
[14] M. García‐ Batlle, O. Baussens, S. Amari, J. Zaccaro, E. Gros‐ Daillon, J.-M. Verilhac, A. Guerrero, G. Garcia‐Belmonte, Moving Ions Vary Electronic Conductivity in Lead Bromide Perovskite Single Crystals through Dynamic Doping, Adv. Electron. Mater. 6 (2020) 2000485. https://doi.org/10.1002/aelm.202000485.
[15] A. Imad, B. Orsal, R. Alabedra, M. Arques, G. Montémont, L. Vergès, EXPERIMENTAL STUDY OF THE CURRENT NOISE SPECTRAL DENSITY VERSUS DARK CURRENT IN CdTe: Cl AND CdZnTe DETECTORS, in: Noise Phys. Syst. 1F Fluct., WORLD SCIENTIFIC, 2001: pp. 335–338. https://doi.org/10.1142/9789812811165_0076.
[16] A. Datta, P. Becla, S. Motakef, Novel Electrodes and Engineered Interfaces for Halide-Semiconductor Radiation Detectors, Sci. Rep. 9 (2019) 9933. https://doi.org/10.1038/s41598-019-46360-z.

Click here to access/download;Figure;Figure1.tif

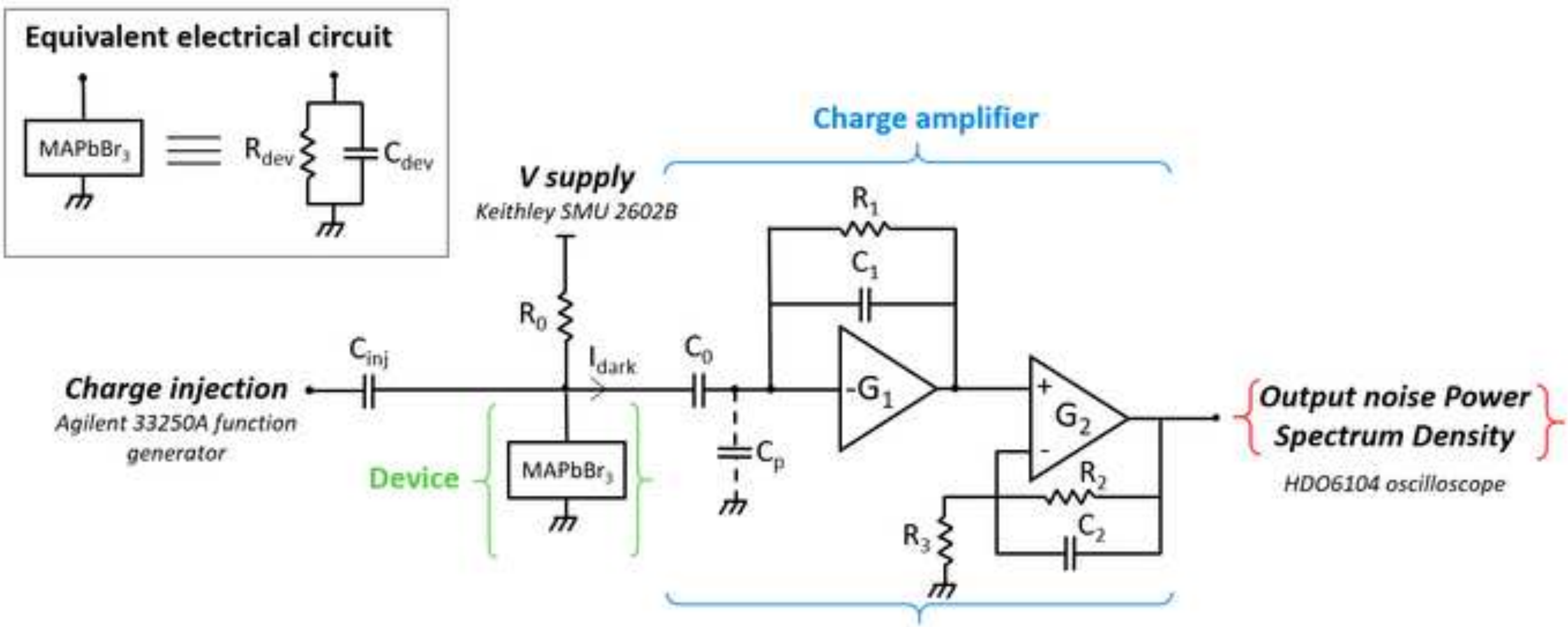

Click here to access/download;Figure;Figure2.tiff

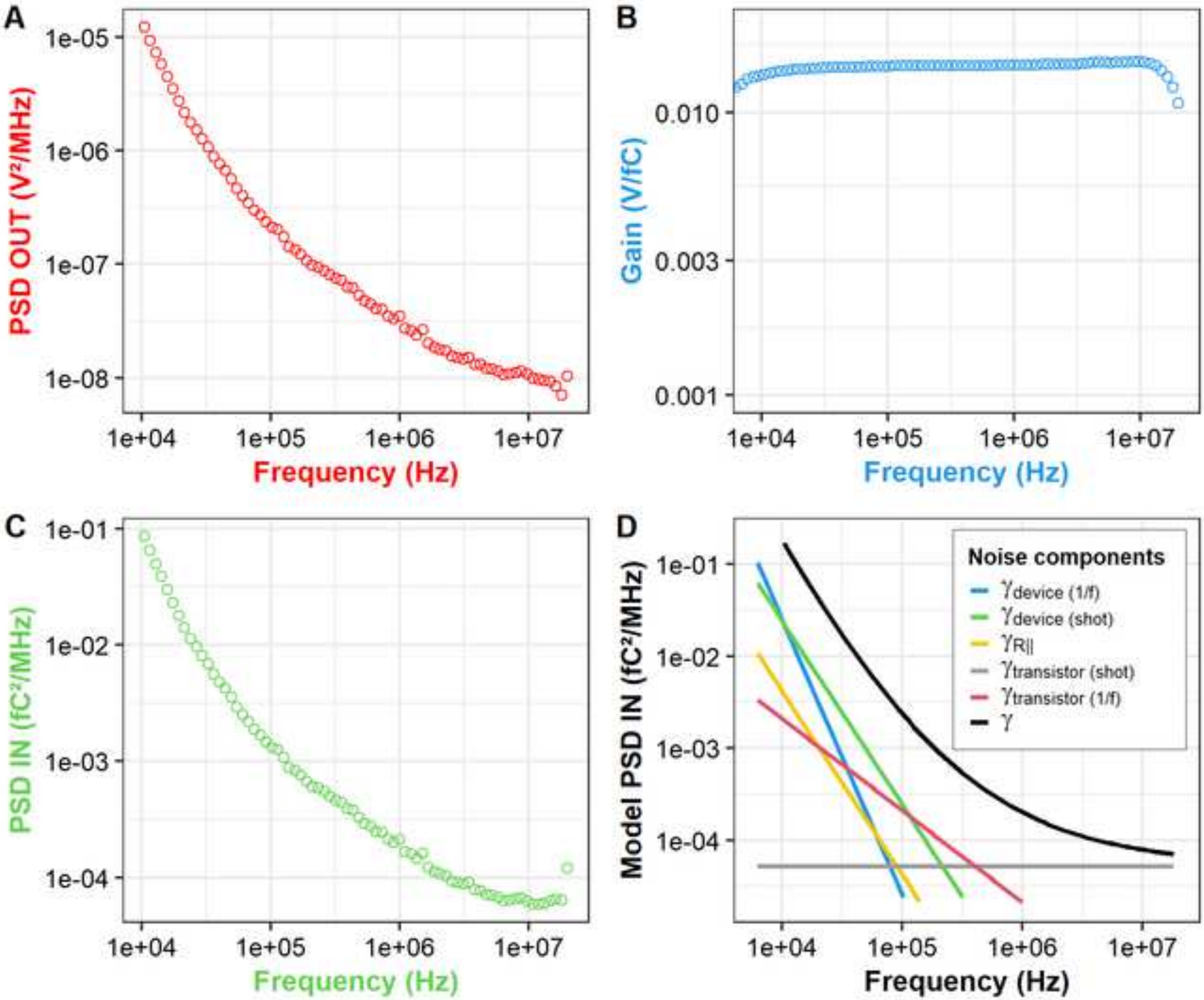

Click here to access/download;Figure;Figure3.tif

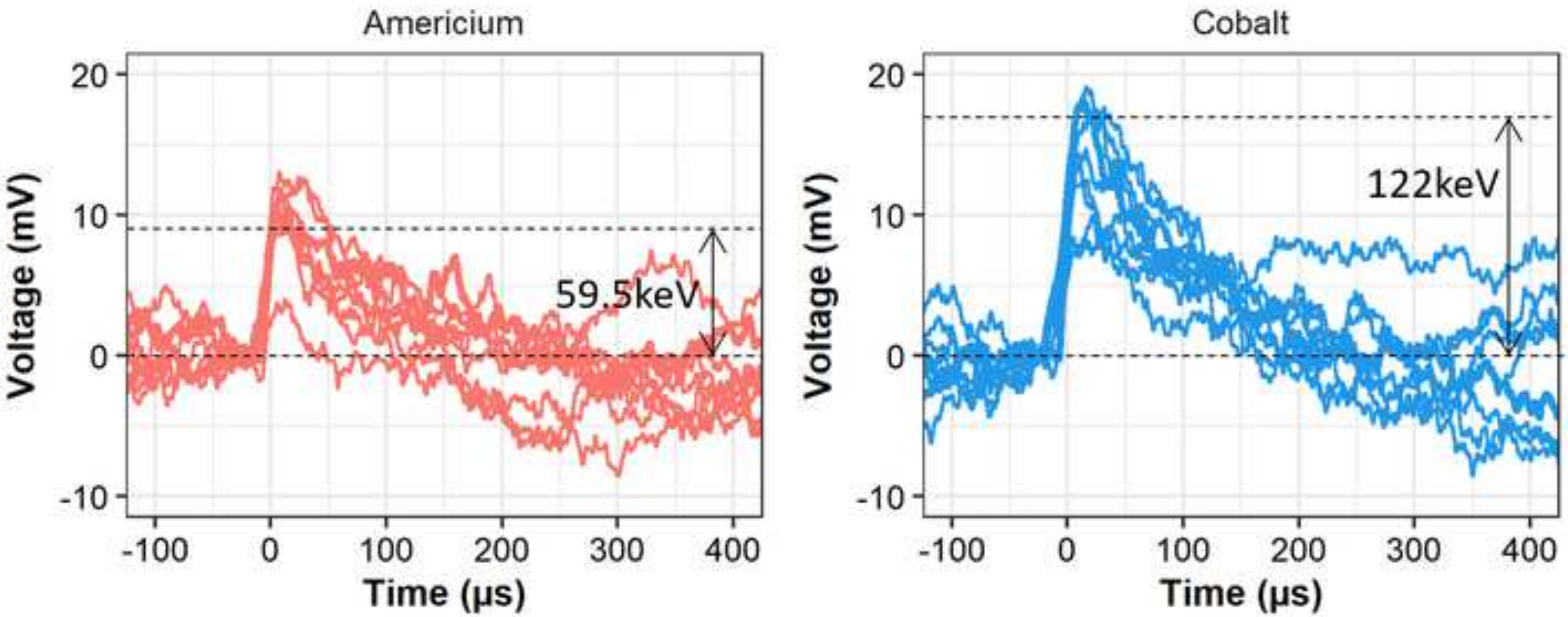

Click here to access/download;Figure;Figure4.tiff

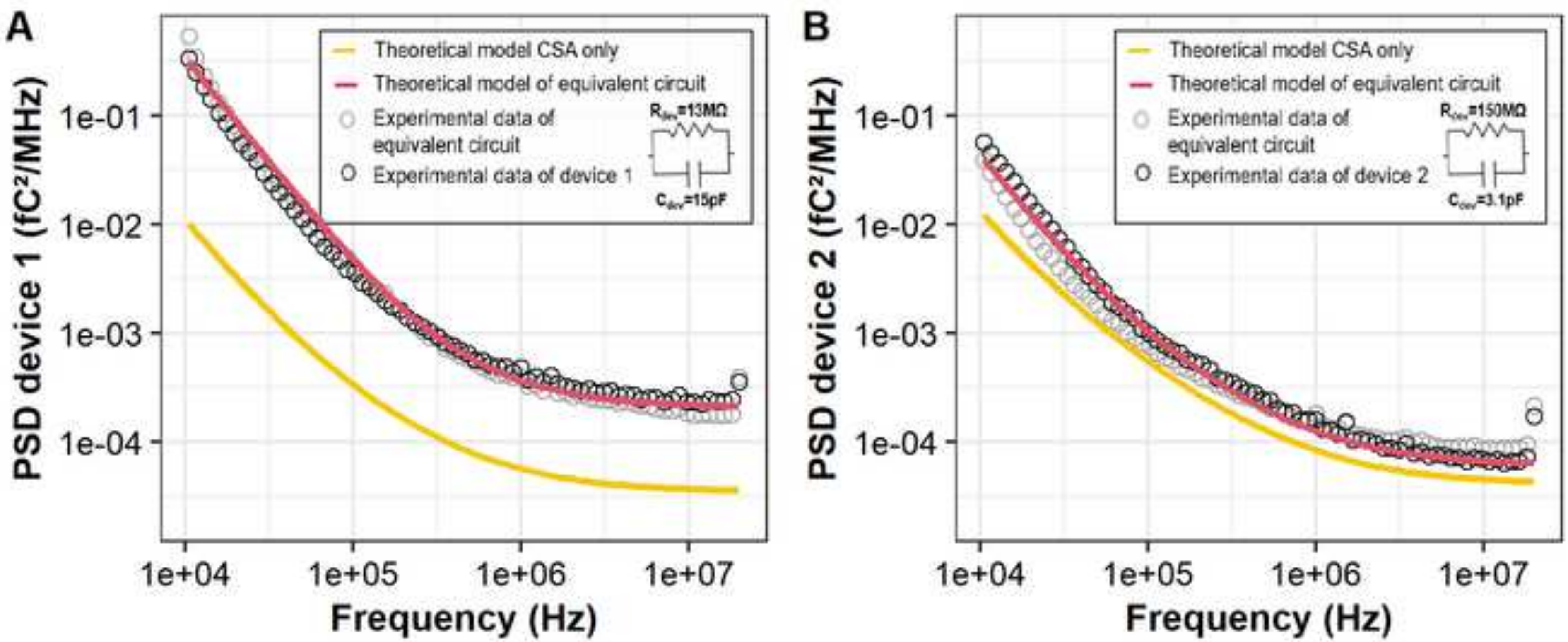

Click here to access/download;Figure;Figure5.tiff

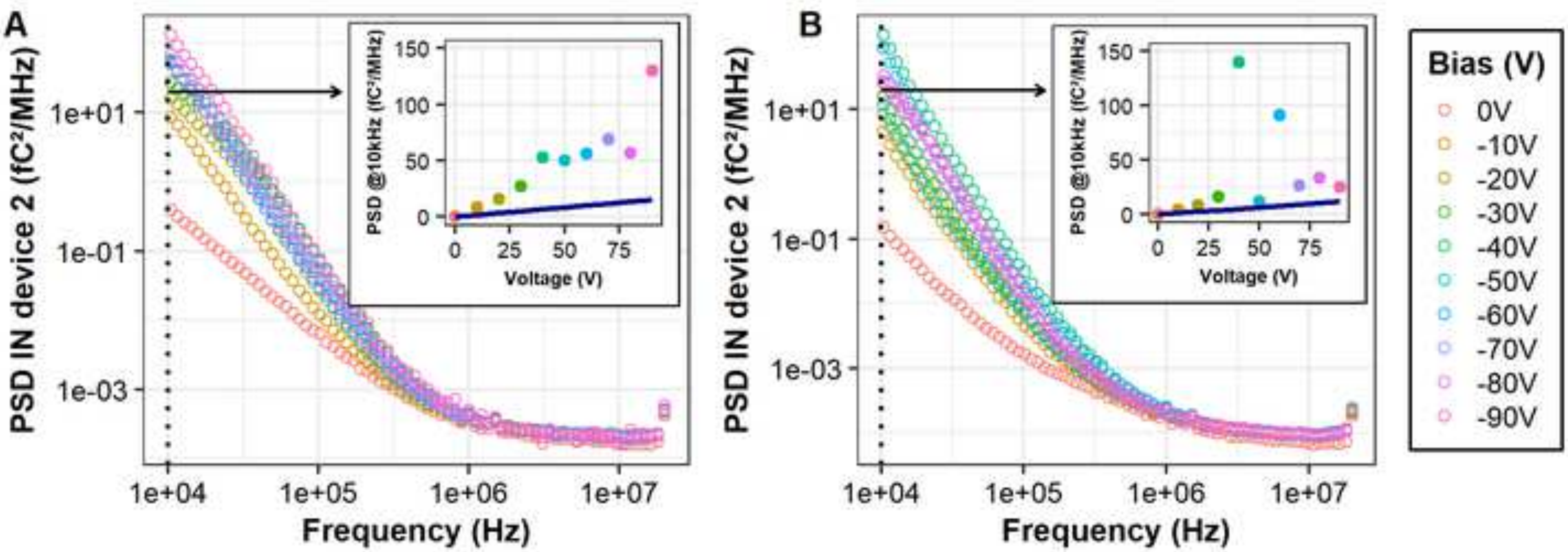

Click here to access/download;Figure;Figure6.tiff

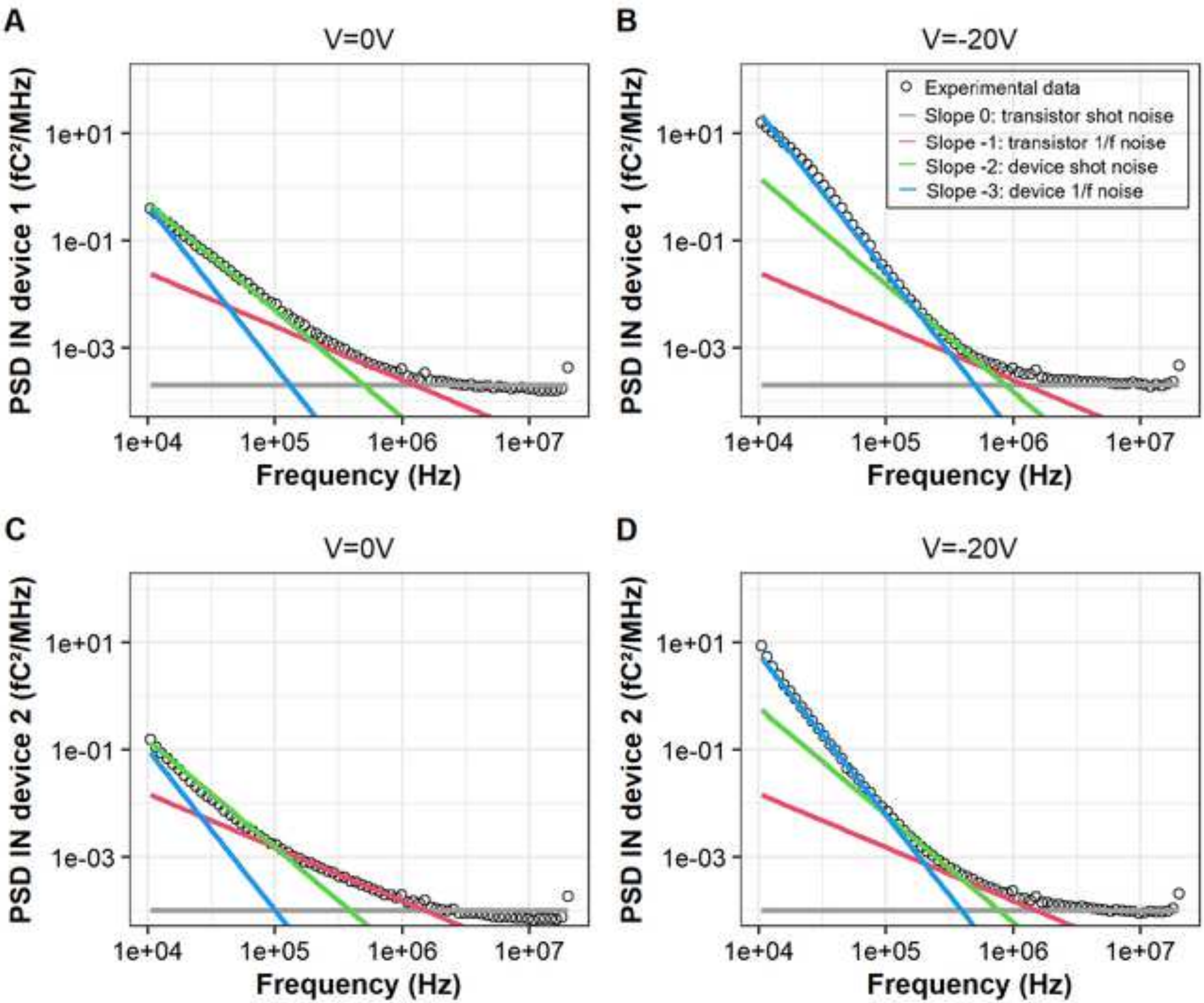

Click here to access/download;Figure;Figure7.tiff

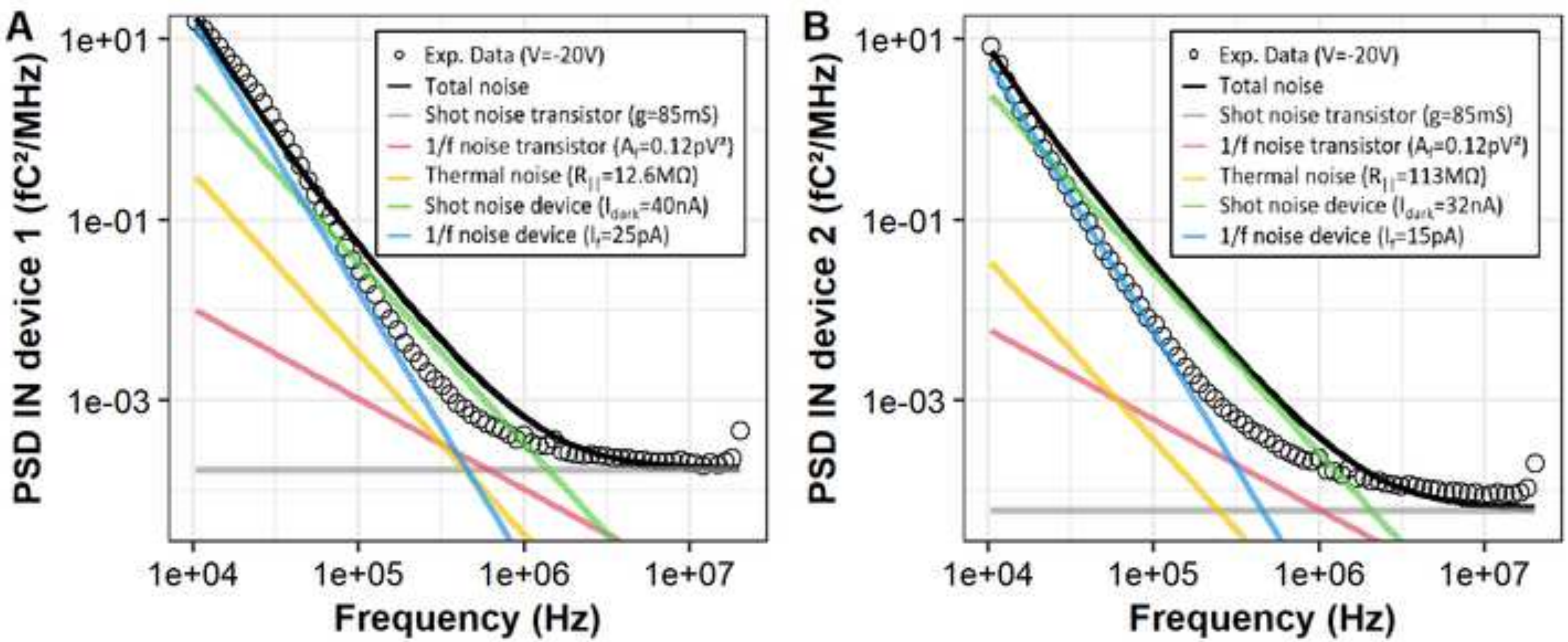

Click here to access/download;Figure;Figure8.tiff

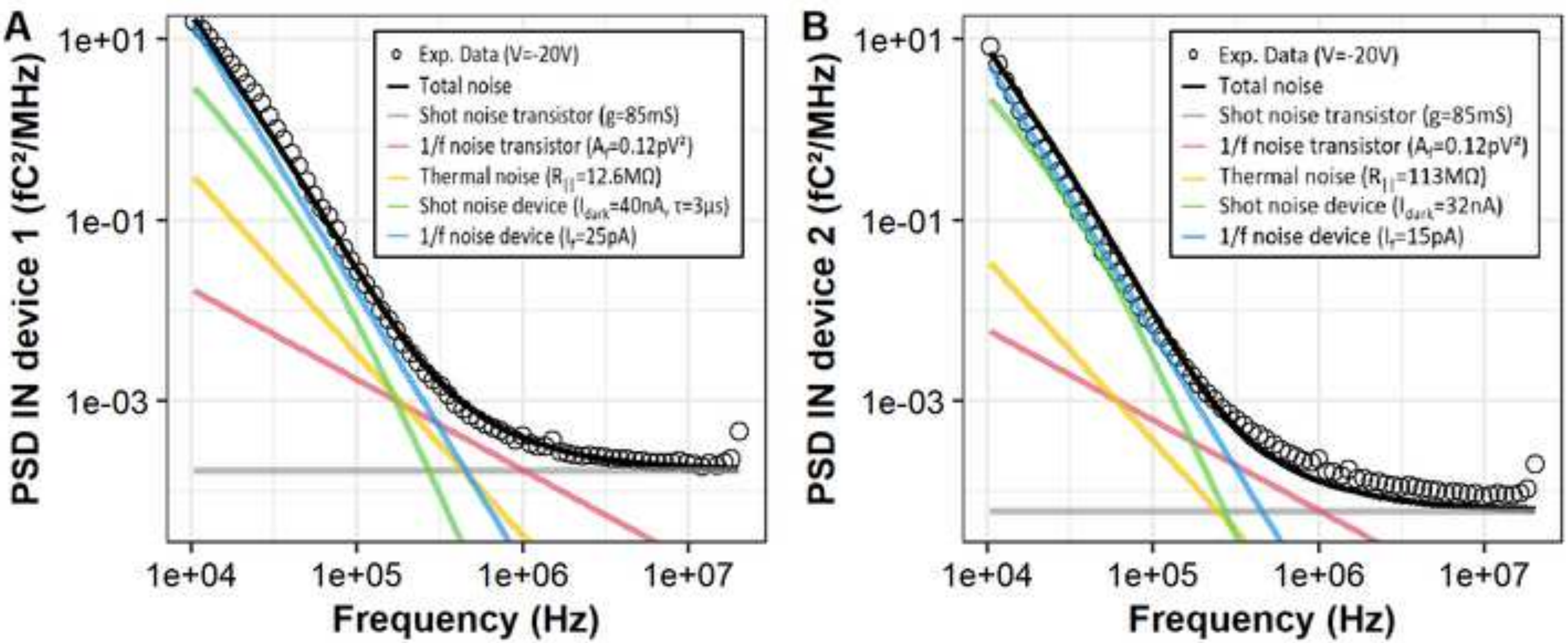

- Electronic noise limits gamma photon counting perovskite devices’ energy resolution
- Low frequency noise of unbiased devices is dominated by resistance thermal noise
- Low frequency noise of biased devices is dominated by dark current 1/f noise

Manuscript

Declaration of interests

☒The authors declare that they have no known competing financial interests or personal relationships that could have appeared to influence the work reported in this paper.

☐The authors declare the following financial interests/personal relationships which may be considered as potential competing interests: